The New Two-Dimensional Electron Gas Base HBT (2DEG-HBT): Two-Dimensional Numerical Simulation

Patrick D. Rabinzohn, Toshiyuki Usagawa, Hiroshi Mizuta, *Member, IEEE*, and Ken Yamaguchi, *Member, IEEE*

Abstract—**The bipolar/FET characteristics of the 2DEG-HBT (Two-Dimensional Electron Gas Base p-n-p AlGaAs/GaAs Heterojunction Bipolar Transistor) are analyzed extensively by a two-dimensional numerical simulator based on a drift-diffusion model. For bipolar operations at high collector current densities, it is confirmed that the cutoff frequency f_T is determined mainly by the collector transit time of holes and by the charging time of the extrinsic base–collector capacitance C_{bc}^{EXT}. The charging times of the emitter and base regions, and the base transit time are shown to be negligible. A high cutoff frequency f_T (88 GHz) and current gain h_{FE} (760) are obtained for an emitter size of 1 × 10 μm^2, an undoped collector thickness of 150 nm, and a collector current density J_c of 10^5 A/cm^2.**

The FET operation of the same 2DEG-HBT structure shows a threshold voltage V_{th} of 0.74 V, the transconductance G_m^{max} of 80 mS/mm, and maximum cutoff frequency f_T^{max} of 15 GHz.

Moreover, the buried SiO_2 structure for reducing the extrinisic base-collector capacitance C_{bc}^{EXT} shows an extremely high cutoff frequency f_T of 163 GHz and maximum oscillation frequency f_{max} of 110 GHz for the bipolar mode. The dependence of the device performance on material parameters is analyzed extensively from a device design point of view. Optimization of the epitaxial layer structure enables the design of a higer performance FET (e.g., G_m = 235 mS/mm and f_T = 19 GHz for L_g = 1 μm) without sacrificing the bipolar function.

I. Introduction

THE 2DEG-HBT (Two-Dimensional Electron Gas Base Heterojunction Bipolar Transistor) [1] is a new functional device, a "bitransistor," operating as both a bipolar transistor and a FET. This bitransistor action is achieved by a new operation principle; the 2DEG at the AlGaAs/GaAs heterointerface acts as either the base of a p-n-p bipolar transistor or the n-channel of a 2DEG-FET [2].

The schematic cross section and the energy-band diagram of the 2DEG-HBT is shown in Fig. 1(a) and (b). The outstanding properties [1] of the proposed 2DEG-HBT are resummarized as follows:

1) Enhanced bipolar performance due to
   a) negligible base transit time of holes due to thin (~ 10 nm) 2DEG base without neutral region,
   b) very low base resistance r'_{bb} due to high electron mobility, especially at low temperatures (77 K).
2) Monolithic integration of 2DEG-FET and p-n-p HBT by the same epitaxial layer structure.
3) Bifunctional operation of bipolar/FET as four-terminal devices.

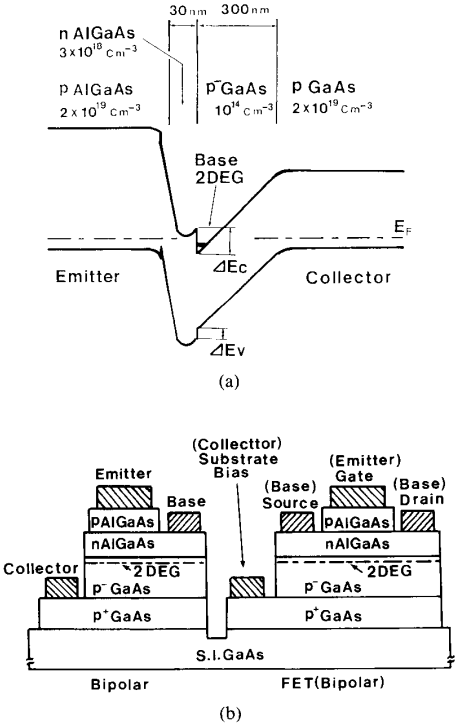

Fig. 1. The conceptual 2DEG-HBT stucture. (a) Energy-band diagram. (b) Cross-sectional view and monolithic integration of p-n-p HBT and 2DEG-FET by the same epitaxial layer structure.

These new concepts offer significant promise. However, at the early stage of device development [1], some key questions arise: what are the actual operating principles and the electrical characteristics of the 2DEG-HBT, particularly as a bipolar transistor, and can the device operate with high performance as a FET and an HBT? This extensive two-dimensional numerical simulation study addresses these questions, confirming the basic principles of the 2DEG-HBT and demonstrating its effective simultaneous operation as a high-performance p-n-p HBT and junction gate 2DEG-FET by the same structure. Guidelines for

Manuscript received May 30, 1990; revised August 20, 1990. The review of this paper was arranged by Associate Editor N. Kawamura.

P. D. Rabinzohn was with Philips Research Organization, L. E. P., Limeil-Brevannes, France. He is now with Matra MHS (Wafer Fab.), CP 3008, 44087 Nantes-Cedex 03, France.

T. Usegawa and K. Yamaguchi are with the Central Research Laboratory, Hitachi Ltd., Kokubunji, Tokyo 185, Japan.

H. Mizuta is with Hitachi Cambridge Laboratory, R & D Centre, Hitachi Europe Ltd., Cavendish Laboratory, Cambridge CB3 OHE, England.

IEEE Log Number 9040646.

device design are given by extensive analysis of the dependence of the device performance on material parameters [3].

Finally we comment on the bifunctional operation, i.e., the simultaneous bipolar and FET actions, and the limitation of the present simulator.

II. Simulated Device Structures

A. Two-Dimensional Heterostructure Device Simulator

The present two-dimensional simulator for heterostructure devices was first developed as an engineering tool for laser diodes called HILADIES (HItachi LAser DIodes Engineering Software) [4], and has recently been extended to the design tool for heterostructure electron devices [5]. This simulator, based on the drift-diffusion classical hydrodynamic model [6], has been successfully applied to the analysis of experimental data from the HEMT device. The differences between the present physical modeling and [5] are as follows:

To model the electron velocity overshoot effect, the drift velocity of electrons is described by the camel-like functional form [6]:

$$V(E) = \frac{\mu_{n0}E + V_s(E/E_c)^4}{1 + (E/E_c)^2} \tag{1}$$

where μ_{n0} is the low-field mobility, V_s the saturation velocity, and E_c the critical field (4×10^3 V/cm). The drift velocity of holes is given by the piecewise linear relation

$$V(E) = \begin{cases} \mu_{p0}E, & E \leq V_s/\mu_{p0} \\ V_s, & E \geq V_s/\mu_{p0} \end{cases} \tag{2}$$

where μ_{p0} is the low-field mobility of holes, the saturation velocity V_s is assumed to be the same for electrons and holes, 10^7 cm/s. A carrier life time of 1 ns is assumed for both electrons and holes ($\tau = \tau_n = \tau_p = 1$ ns) unless otherwise specified [4], [5]. We have also introduced a single donor level *DX* center model as shown in Table I to describe the deep donor density in n-AlGaAs [3], [5].

The material parameters for GaAs, AlGaAs are listed in Table I. The other mathematical formulas, notations, material parameters, etc., can be found in [4], [5].

B. Simulated "Central" Device Structures

The 2DEG-HBT structure modeled in this work is shown in Fig. 2. In this work, one of the main concerns is the bipolar/FET operation by the same structure; the source electrode and the drain electrode also act as the two base electrodes. The simulated device width and the emitter size are fixed at 10 μm and 1×10 μm^2, respectively. From an intuitive understanding of the 2DEG-HBT operation, we have defined the "central value" of material parameters for the simulated 2DEG-HBT structure, as specified in Table II.

The simulated device structure (Fig. 2) is a self-aligned structure of the emitter region, the emitter electrode, and the n^+ GaAs base contact regions (layers IX), based on a fabricating self-alignment process. The thickness of layers IX is equal to the sum of the thicknesses of layers I to VI. Finally, SiO_2 sidewall spacers (layers *X*; 0.15 μm thick) provide isolation between the base regions and the emitter and metallugical base; that is, the sidewalls extend to a depth equal to the thickness of layers I to IV. Thus connection to the base, the 2DEG at the AlGaAs/GaAs interface, is at the contact between n^+ GaAs (IX) and layers V and VI.

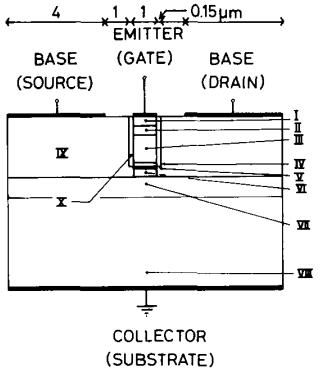

Fig. 2. The simulated 2DEG-HBT structure. The layer structure is described in Table II.

TABLE I
PHYSICAL PARAMETERS OF $Al_xGa_{1-x}As$ MATERIALS FOR $x \leq 0.45$ AND $T = 300$ K

Parameter	Formula
Dielectric constant	$\epsilon_r = 13.1 - 3.0X$
Electron affinity (eV)	$\chi = 4.07 - 0.6(E_g^\Gamma(x) - E_g^\Gamma(0))$
Bandgaps	
E_g^Γ (eV)	$E_g^\Gamma = 1.422 + 1247X$
E_g^L (eV)	$E_g^L = 1.707 + 0.642X$
E_g^X (eV)	$E_g^X = 1899 + 0.125X + 0.143X$
Electron mass	
m_e^Γ/m_0	$m_e^\Gamma/m_0 = 0.067 + 0.083X$
m_e^L/m	$m_e^L/m_0 = 0.55 + 0.12X$
m_e^X/m_0	$m_e^X/m_0 = 0.85 - 0.07X$
Hole mass m_h/m_0	$m_h/m_0 = 0.48 + 0.31X$
DX center level ΔE_D(meV)	$\Delta E_D = 4 \quad 0 < X < 0.25$ $= 1125X - 277.25, \quad 0.25 < X < 0.37$ $= -261.54X + 235.77, \quad 0.37 < X < 0.45$

TABLE II
MATERIAL PARAMETERS FOR THE SIMULATED "CENTRAL" DEVICE STRUCTURES OF THE 2DEG-HBT

Layer	Material	Al Fraction	Thickness (nm)	Doping Density (cm^{-3})
I	p-GaAs		50	10^{20}
II	p-GaAs		50	5×10^{19}
E III	p-AlGaAs	$X_E = 0.45$	150	$N_E = 10^{19}$
B IV	n-AlGaAs	$X_B = 0.3$	25	$N_B = 2 \times 10^{18}$
V	p-AlGaAs	$X_B = 0.3$	6	10^{14}
VI	p-GaAs		40	10^{14}
			$W_C =$ {	
C VII	p-GaAs		110	10^{14}
VIII	p-GaAs		490	10^{19}
IX	n-GaAs			3×10^{18}
X	SiO_2			

For the sake of comparison with typical p-n-p HBT's, the revised p-n-p HBT structure from Sunderland *et al.* [7] was analyzed as a reference. This p-n-p HBT is described with the help of Fig. 2 and Table II; the metallurgical base (layer IV) and its spacer layer (layer V) are replaced by n-GaAs (30 nm, 3×10^{18} cm^{-3}) and the lightly doped collector consists of layer VI (40 nm, 10^{16} cm^{-3}) and layer VII (400 nm, 10^{16} cm^{-3}). The other device parameters are the same with the central values as shown in Fig. 2.

The current gain h_{FE} is derived from the variations of the ratio $\Delta I_C/\Delta I_B$ of collector current (ΔI_C) to base current (ΔI_B). The static current gain $\beta = I_C/I_B$ is used in the final section to discuss the parasitic resistance.

The delay time associated with one region X of the device is given by

$$\tau_x = \left.\frac{\Delta Q_x}{\Delta I_C}\right|_{V_{CE}} \tag{3}$$

where ΔQ_x is the incremental excess charge in region X of the simulated device structure, and defined by

$$\Delta Q_x = W\Delta\left(\int\int q(n - n_0)\,dx\,dy\right) \tag{4}$$

where W denotes the transistor width of 10 μm and n_0 represents the carrier density in equilibrium. The cutoff frequency is given by

$$f_T = \left.\frac{1}{2\pi}\frac{\Delta I_C}{\Delta Q}\right|_{V_{CE}} \tag{5}$$

where ΔQ is the incremental excess charge in the whole simulated device. The device transconductance is calculated by

$$G_m = \left.\frac{\Delta I_C}{\Delta V_{BE}}\right|_{V_{CE}}. \tag{6}$$

III. Operating Principles

This section concentrates on the device analysis of the "central structure" specified by Table II, to confirm the basic operating principles of the 2DEG-HBT. The specific p-n-p HBT mentioned earlier is also analyzed for comparison.

A. Static Characteristics

The collector and base currents of the p-n-p HBT and the 2DEG-HBT are plotted in Fig. 3(a) as functions of the emitter–base voltage. The collector current has a similar slope for both devices, with an ideality factor of 1.1. Nevertheless, to obtain the same collector current, the emitter–base junction of the 2DEG-HBT must be forward-biased by 0.2 V more than the p-n-p HBT, i.e., the collector saturation current of the 2DEG-HBT appears to be smaller (500 times). Fig. 3(a) also shows the same ideality factor for the base current of both devices, that is, 1.7 for most of the emitter–base voltage range. Therefore, electron–hole recombination, rather than electron injection into the emitter, dominates the base current of p-n-p HBT's. This is in contrast with the abrupt n-p-n HBT's (see for example [6]).

Thus as shown in Fig. 3(b), the common emitter current gain h_{FE} increases with the collector current density J_C until the high injection state is reached. The maximum current gains of 760

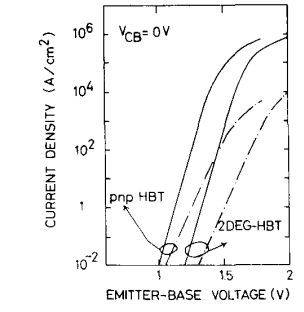

(a)

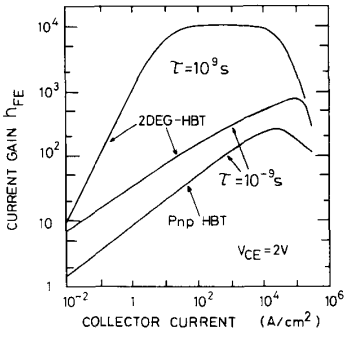

(b)

Fig. 3. Static characteristics of the 2DEG-HBT defined by Fig. 2 and Table II, and the p-n-p HBT specified in the last part of Section II. (a) Collector (solid line) and base (dashed line) currents versus emitter–base voltage. (b) Common emitter current gain h_{FE} versus collector current density, with the carrier lifetime as a parameter.

for the 2DEG-HBT and 280 for the p-n-p HBT are achieved at 10^5 A/cm^2 and 2×10^4 A/cm^2, respectively. The higher current gain of the 2DEG-HBT arises from a smaller recombination current.

Since the hole and electron lifetimes were assumed to be equal (τ = 1 ns) for SRH-type recombination, the wider bandgap metallurgical base of the 2DEG-HBT accounts for the much smaller base current. To confirm the importance of the recombination current, the 2DEG-HBT characteristics shown in Fig. 3(b) were also computed with an artificially long carrier lifetime ($\tau = 10^9$ s) in all layers. Thus by removing the recombination component, the ideality factor of the base current approaches unity and the h_{FE}–J_C curve shows a plateau. The current gain is increased more than tenfold. By setting $\tau = 10^9$ s only in layer IV (n-AlGaAs), such a gedanken simulation also establishes that recombination mostly takes place in n-AlGaAs because it coincides with the the h_{FE}–J_C curve of the above structure with the artificial long carrier life times in all layers.

The carrier concentration profiles are shown in Fig. 4 for the same collector current density. The carrier profile of the p-n-p HBT indicates a neutral base region. On the other hand, the 2DEG-HBT has no neutral base for a forward-biased emitter–base diode. Moreover, the base region is completely depleted of carriers under when not biased. As the n-AlGaAs layer shown in Fig. 4 is not as completely depleted as when biased, the residual electrons in the n-AlGaAs may also act as the base. However, electron injection from n-AlGaAs into the emitter is

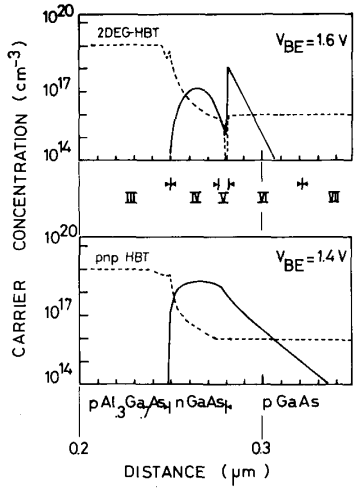

Fig. 4. Electron (solid line) and hole (dashed line) concentration profiles versus distance from the surface in the vicinity of the base, for a collector density of 10^4 A/cm^2.

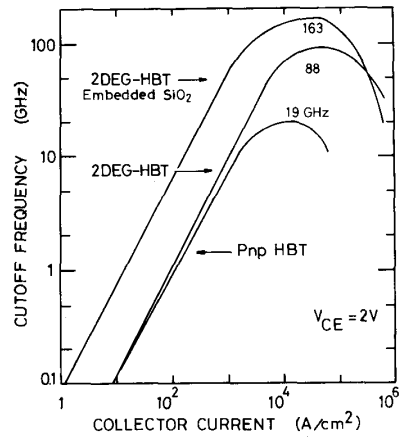

Fig. 5. Cutoff frequency f_T versus collector current density J_C for the p-n-p HBT, the 2DEG-HBT, and the embedded SiO_2 structure of the 2DEG-HBT.

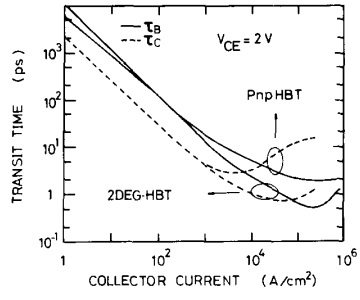

Fig. 6. Base (solid line) and collector (dashed line) delay times versus collector current density for the 2DEG-HBT and p-n-p HBT.

suppressed as shown, by designing the emitter layer with a larger Al mole fraction of p-AlGaAs than the metallurgical n-AlGaAs base. Nevertheless, this is not a necessary condition for the 2DEG-HBT to show gain enhancement with respect to the homojunction transistor, as discussed in Section IV. Thus by applying the principle of modulation doping to the base of a bipolar structure, a device without neutral base is truely achieved. The metallurgical base can be considered to be the emitter–base transition layer rather than the actual base (Fig. 4). Therefore, high-frequency and/or high-speed operation is expected as the base transit time is not limited.

B. Frequency Performance Analysis

Fig. 5 plots the cutoff frequency f_T against the collector current density J_C for the 2DEG-HBT and the p-n-p HBT. The maximum cutoff frequencies f_T are 88 GHz at $J_C = 4 \times 10^4$ A/cm^2 for the 2DEG-HBT, and 19 GHz at $J_C = 10^4$ A/cm^2 for the p-n-p HBT. The difference in f_T results from the different base and collector delay times τ_B and τ_C due to the different structures. This is discussed later. The detailed analysis of the f_T–J_C curve is performed by subdivision into regional delay times τ_x, as defined by (3). The emitter region E consists of p-GaAs (layers I and II) and p-AlGaAs (layer III). The base region B consists of n-AlGaAs metallurgical base (layer IV), p-AlGaAs spacer (layer V), and n^+ GaAs base contact regions (layers IX). The collector region C consists of p-GaAs (layers VI, VII, and VIII). The analysis of the regional delay times is shown in Fig. 6.

First, it is striking that the delay time associated with the emitter of both devices is always negligible, rising almost linearly with current density to 0.1 ps for the 2DEG-HBT and 0.02 ps for the p-n-p HBT. In contrast with the conventional design of n-p-n HBT's, the emitter doping level of both devices exceeds the base doping level. Thus the emitter–base transition capacitance charging time would appear in this analysis as a component of the base delay time rather than the emitter delay time for the ongoing analysis. Therefore, the emitter delay time, as defined here, is due to the injection of electrons from the base into the emitter, which is so small, that the delay time encountered by minority carriers flowing from emitter to collector is shared by the metallurgical base and collector layers.

The basic principle of the 2DEG-HBT is better understood by comparing the delay times of the two devices at high current densities. The minimum base delay time τ_B of the p-n-p HBT is observed to be 2 ps, which can be roughly estimated by the classical formula for the base delay time $\tau_B = W_b^2/2D_p$ with W_b = 30 nm and D_p = 3.1 cm^2/s for the 3×10^{18} cm^{-3} n-GaAs base. On the other hand, the minimum base delay time τ_B of the 2DEG-HBT is 0.6 ps, due to the absence of a neutral base (Fig. 4). The minimum computed collector delay times τ_C for the p-n-p HBT and the 2DEG-HBT are 3.0 and 0.75 ps, respectively, which also can be roughly estinated by a simple formula for the base–collector depletion layer transit time $X_d/2V_s$ where X_d denotes the collector depletion layer width, about 440 nm for the p-n-p HBT and 150 nm for the 2DEG-HBT.

For a more detailed analysis of the 2DEG-HBT, the regional delay time τ_x is divided into the intrinsic part τ^{int} and the extrinsic part τ^{ext}.

The intrinsic device is the central 1 μm × 10 μm region of Fig. 2. The intrinsic delay time consists of the emitter–base depletion layer (layer IV) delay time τ_{be}^{int}, the delay time τ_b^{int} of layer V, and the base–collector depletion layer (layers VI and

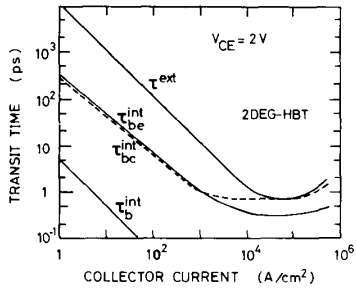

Fig. 7. Extrinsic base-collector charging time τ^{ext} (solid line) and intrinsic components of the delay time τ^{int}_{be} (layer IV), τ^{int}_{b} (layer V), and τ^{int}_{bc} (layers VI and VII, dashed line) versus collector current density for the structure of Fig. 2 and Table II.

VII) delay time τ^{int}_{bc}. Such regional analysis of the delay times is shown in Fig. 7.

At low collector current densities, the delay time is dominated by the extrinsic delay time τ^{ext}, which can be estimated accurately by the ratio of a 110-fF extrinsic base-collector capacitance, in agreement with the geometric capacitance of the extrinsic part of layer VII, to the transconductance ($G_m = qI_C/kT$).

The 2DEG-HBT achieves its minimum delay time at the high current density of 4×10^4 A/cm^2. In this case, the 1.8-ps computed delay time in Fig. 7 consists of τ^{ext} (= 0.75 ps), τ^{int}_{be} (= 0.3 ps), and τ^{int}_{bc} (= 0.75 ps). Even at these large collector current densities, the extrinsic charging time τ^{ext} is given accurately by the ratio of capacitance (110 fF) to transconductance (150 mS).

The intrinsic emitter-base transit time τ^{int}_{be} and the base-collector depletion layer transit time τ^{int}_{bc} are well explained by the following simple formulas:

$$\tau^{int}_{be} = W_{IV}/V_s = 0.25 \text{ ps} \quad (7)$$

$$\tau^{int}_{bc} = W_C/2V_s = 0.75 \text{ ps} \quad (8)$$

where W_{IV} is the thickness of layer IV and W_C is the thickness of the lightly doped collector (layers VI and VII). Assuming a triangular concentration profile for the holes in n-AlGaAs (layer IV), as suggested in Fig. 4, and the saturation velocity for the motion of holes through n-AlGaAs, τ^{int}_{be} can be represented by (7).

As shown by the regional analysis of the delay times in Fig. 7, reducing the extrinsic base-collector capacitance C^{EXT}_{bc} is one of the main issues for realizing the high-performance 2DEG-HBT. Therefore, an embedded SiO_2 structure was simulated by replacing the extrinsic part of the collector layer VII–VIII (Fig. 2) by SiO_2. The computed cutoff frequency f_T versus collector current density is shown in Fig. 5 with a maximum cutoff frequency of 163 GHz, that is, a minimum delay time of 1 ps, which approaches the intrinsic device performance.

C. FET Characteristics

One of the distinct advantages of the 2DEG-HBT is the monolithic integration of high-speed p-n-p transistors and n-channel FET's by the same epitaxial layer structure. From the FET operation point of view, the 2DEG-HBT is basically a p-AlGaAs gate 2DEG-FET with a p-GaAs buffer layer.

To our knowledge, the 2DEG-HBT is the first device with this promising property. The Bipolar Inversion Channel FET

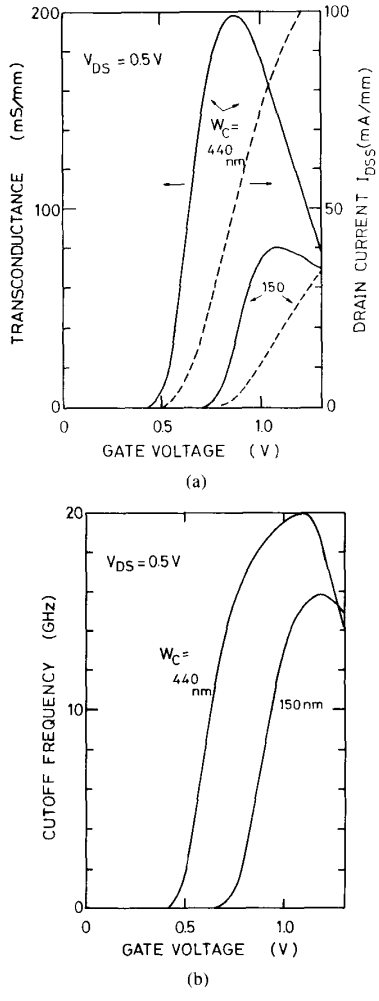

Fig. 8. FET characteristics of the 2DEG-HBT with W_C (Table II) as a parameter. (a) Transconductance (solid line) and drain saturation current (dashed line) versus gate voltage. (b) Cutoff frequency versus gate voltage.

(BICFET) [8] could in principle be considered similarly, but, it has so far been restricted to its bipolar operation, probably to simplify fabrication. Hence the BICFET designed with a planar three terminal (Source, Emitter, Collector) structure has shown serious current crowding problems [9]. On the contrary, the 2DEG-HBT is designed as a four-terminal device, i.e., p-AlGaAs emitter (gate), p-GaAs collector (substrate), and two contacts (source and drain) to the 2DEG base (or n-channel).

The central structure of the 2DEG-HBT, shown in Fig. 2 and Table II, is simulated as a junction-gate FET with a p-GaAs buffer layer. The FET characteristics (transconductance G_m, gate capacitance C_G, and cutoff frequency f_T) are simulated by the same definitions as in [5].

The transconductance G_m, the source-drain saturation current I_{DSS}, and the cutoff frequency f_T are shown in Fig. 8(a) and (b) for the central structure (W_C = 150 nm) and the wider collector structure (W_C = 440 nm). The difference between the FET performances comes from the fact that the built-in potential from the collector p-GaAs (layer VIII) reduces the 2DEG sheet density.

IV. Influence of the Device Parameters

To investigate the dependence of the device performance on the material parameters, each device parameter was individually varied from the "central value" in Fig. 2 and Table II. Simulations were performed changing the Al mole fraction, the doping level, and the thicknesses of the emitter (layer III), metallurgical base (layer IV), and collector (layer V–VI).

A. Emitter and Base Al Mole Fraction

As stated before, the primary effect of designing the p-AlGaAs emitter layer (III) with a higher Al mole fraction than the n-AlGaAs base layer (IV) is to prevent electron injection from the n-AlGaAs into the emitter. Hence the base current is reduced to its recombination component. This is shown by the current gain–collector current density (h_{FE}–J_C) curve in Fig. 9. In contrast with the device reported so far (emitter Al content $X_E = 0.45$), the 2DEG-HBT with $X_E = X_B = 0.3$ shows a flat current gain, that is, a base current ideality factor close to unity. Therefore, electron injection into the emitter reduces the maximum current gain to 115. However, this h_{FE} is still twice that of the homojunction $Al_{0.3}Ga_{0.7}$. As p-n-p bipolar transistor and ten times larger than that of the GaAs p-n-p bipolar transistor. This result is in qualitative agreement with the basic principle of the 2DEG-HBT.

The cutoff frequency–collector current density characteristics of the 2DEG-HBT with $X_E = 0.3$ is similar to that of Fig. 5 ($X_E = 0.45$) but saturates at 54 GHz, that is, $\tau_{be}^{int} = 0.55$ ps and $\tau_{bc}^{int} = 1.35$ ps. This can be explained by a hole velocity smaller than the saturation velocity obtained for $X_E = 0.3$. Hence the emitter–base heterojunction may also act as a hot hole launcher.

The maximum gain h_{FE}^{max} of the 2DEG-HBT and the current density associated with this h_{FE}^{max} are plotted in Fig. 10 as functions of the n-AlGaAs Al mole fraction X_B. The h_{FE}^{max}–X_B curve is strongly correlated with the dependence of X_B on the deep donor (i.e., *DX* center) energy ΔE_D (Table I). As ΔE_D increases, the ionized donor density as well as the free electron concentration in n-AlGaAs decrease. This reduces the recombination current. The importance of the *DX* centers to the base current was also checked by simulating the 2DEG-HBT ($X_B = 0.3$) with a fully ionized impurity model. As shown in Fig. 10, the computed value of h_{FE}^{max} is 215 instead of 760 for the deep donor model. The reported correlation mentioned above and the band diagram suggests that the electron quasi-Fermi level is pinned at the deep donor energy.

In contrast with the dc characteristics, the cutoff frequency of the 2DEG-HBT is constant for X_B between 0.2 and 0.4.

B. Emitter and Base Doping Level

The h_{FE}–J_C curve is shown in Fig. 11 with the emitter doping level N_E as a parameter. For emitter doping less than 10^{18} cm^{-3}, electron injection into the emitter dominates. Moreover, the emitter series resistance limits the current-handling capability. The corresponding low value of the device transconductance, 40 mS, also reduces the maximum cutoff frequency to 39 GHz. It is therefore highly desirable to design the emitter with a higher doping level than the base, as for any bipolar transistors. However, this design principle is usually modified for n-p-n HBT's [10], mostly because of the limited doping level achievable for n-AlGaAs. One of the advantages of p-n-p GaAs HBT's over n-p-n GaAs HBT's is the high doping capability of the emitter region.

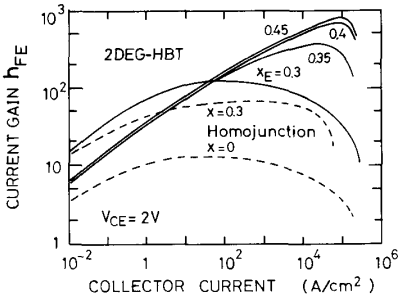

Fig. 9. Common emitter current gain versus collector current density for the 2DEG-HBT (solid line) with the emitter Al content X_E as a parameter. The dashed lines are for p-n-p homojunction transistors with Al contents $X = 0.3$ and 0.0. Other parameters are as in Table II.

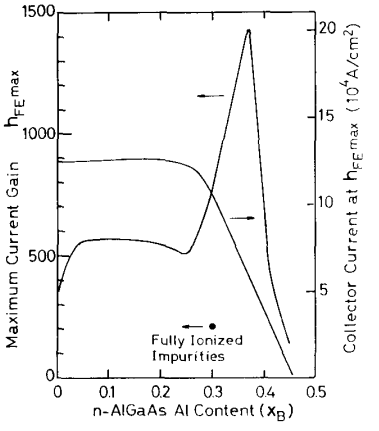

Fig. 10. Maximum current gain h_{FE}^{max} and corresponding collector current density versus n-AlGaAs Al content X_B. Other parameters are as in Table II. The dark point ● was calculated with a fully ionized impurity model for $X_B = 0.3$.

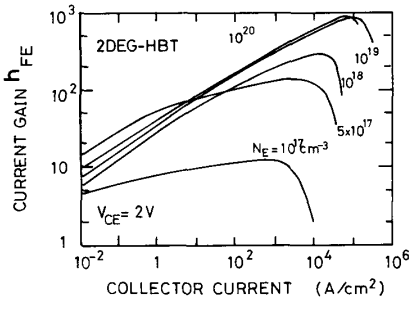

Fig. 11. h_{FE}–J_C characteristics of the 2DEG-HBT with the emitter N_E (layer III) doping level as a parameter. Other parameters are as in Table II.

Fig. 12 plots the h_{FE}–J_C characteristic with the n-AlGaAs doping level N_B of the metallurgical base as a parameter. At low doping levels, the computed current gain appears to be as high as 10^5 for a small emitter–base forward bias. This phenomenon is accompanied by a large collector current showing an ideality factor of around 15. In this condition the device could be described as a punchthrough diode. For the enhancement-

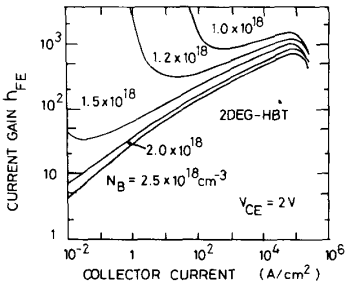

Fig. 12. h_{FE}–J_C characteristics of the 2DEG-HBT with the metallurgical base (layer IV) doping level N_B as a parameter.

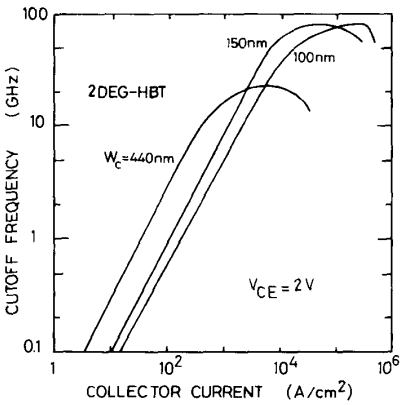

Fig. 13. f_T–J_C characteristics of the 2DEG-HBT with the lightly doped collector thickness W_C as a parameter.

type 2DEG-HBT reported here, this phenomenon always exists, e.g., only at very small current densities for the structure of Table II. The low doping limit of the metallurgical base, n-AlGaAs, is similar to that of devices such as the Bipolar Inversion Channel FET (BICFET) [8] or the Inversion Base Transistor (IBT) [11]. In this case, even though an extremely large current gain h_{FE} is expected at low collector current densities, this simulation results show that the emitter and collector will be in the punchthrough state.

In the investigated range of N_B ($1\text{–}3 \times 10^{18}/cm^3$), the cutoff frequency is not affected at high current densities, above 10^3 A/cm^2. However, the rise of f_T with J_C is steeper with the punchthrough effect.

C. Collector Thickness

The h_{FE}–J_C curve of the 2DEG-HBT is unchanged at low current by variations in the lightly-doped collector (layers VI and VII) width W_C. The only effect of increasing W_C is a reduction in the current density at which h_{FE} starts to fall; this is attributed to the Kirk effect. Thus a smaller h_{FE}^{max} is observed, e.g., 380 for $W_C = 440$ nm.

The cutoff frequency characteristics of the 2DEG-HBT are given in Fig. 13 for $W_C = 100$, 150, and 440 nm. The shift of the curve toward lower current densities as W_C increases indicates that the extrinsic base-collector capacitance is reduced. For $W_C = 440$ nm, f_T saturates at 23 GHz as the intrinsic base-collector transit time τ_{bc}^{int} increases to 5 ps. From the device design point of view, this cutoff frequency of the 2DEG-HBT with the $W_C = 440$ nm structure should be compared with the reference p-n-p HBT which has a maximum f_T of 19 GHz defined by the last part of Section II. For $W_C = 100$ nm, the improvement in τ_{bc}^{int} is balanced by an increase in τ_{be}^{int} (1 ps). Thus f_T shows a small improvement at most: 92 GHz compared to 88 GHz for $W_C = 150$ nm.

D. FET Characteristics and Bifunctional Operations

For the FET operation of the 2DEG-HBT, the main points of interest are the effects of the p-buffer layer and p-n junction gate on the FET performance.

In the normal design of 2DEG-HBT, the p-AlGaAs gate doping level N_E is much larger than the n-AlGaAs doping level N_B. However, a decrease in the gate doping level to $N_E = 1 \times 10^{18}/cm^3$ strongly affects the device performance; the threshold voltage V_T becomes -0.55 V (depletion-type FET) and the maximum transconductance G_m^{max} falls to 55 mS/mm. When the p-AlGaAs gate doping level N_E is smaller than the n-AlGaAs doping level N_B, the depletion layer extends more deeply into the p-AlGaAs layer so that the FET performance degrades further.

The characteristics of the FET operation of the 2DEG-HBT are given in Fig. 14(a) and (b) with the n-AlGaAs doping level N_B as a parameter. The threshold voltages V_T are 0.04, 0.74, and 0.89 V for $N_B = 3$, 2, and $1.2 \times 10^{18}/cm^3$, respectively. G_m and f_T are unchanged by increasing N_B from 2 to $3 \times 10^{18}/cm^3$. Most importantly, the donor neutralization process has a decreasing influence on the formation of 2DEG, as the doping level is lowered below $2 \times 10^{18}/cm^3$. Thus a higher maximum transconductance (235 mS/mm) and cutoff frequency (19 GHz) are obtained for $1.2 \times 10^{18}/cm^3$.

The 2DEG-HBT is the first device to operate simultaneously as a FET and a bipolar. The bifunctional mode is obtained by biasing both the gate (or emitter) and the drain (or right-hand side base). We first consider the effect of a large applied gate voltage on the FET characteristics for the embedded SiO_2 structure. The source-drain saturation current I_{dss} and the transconductance G_m are shown in Fig. 15(a) as functions of the gate voltage. For $V_G \geqq 1.9$ V, the transconductance G_m reaches a plateau of 2.4 S/mm. In this region, the source supplies additional electrons to electrically neutralize the large number of holes injected into the heterointerface. The carrier concentration profiles computed for $V_G = 2$ V explain this situation in Fig. 15(b). The gate capacitance also steadily increases; the corresponding cutoff frequency f_T has a peak value of 7.5 GHz for $V_G = 1.9$ V.

Regarding the bifunctional operation, biasing the drain with respect to the source enables injection of electrons into the channel in excess of the equilibrium 2DEG density. Charge neutrality is maintained because of the large hole flow perpendicular to the electron flow. Consequently, a neutral charge region with negligible electric field is formed in the lightly doped p-GaAs layer.

The current characteristics are very similar to the bipolar I–V curves of Fig. 3(a), with ideality coefficients of 1.15 and 1.50 for the collector and base currents, respectively. Indeed, with the preceding definition of the base current, the collector and base currents obtained for $V_{DS} = 0.5$ V and $V_{BE} = X$ V are exactly equal to the collector and base currents computed for $V_{DS} = 0$ V, $V_{BE} = X - 0.12$ V. Hence, the h_{FE}–J_C characteristics remain unchanged by applying a drain bias. The f_T–J_C curve is also similar to that of the bipolar mode (no drain bias)

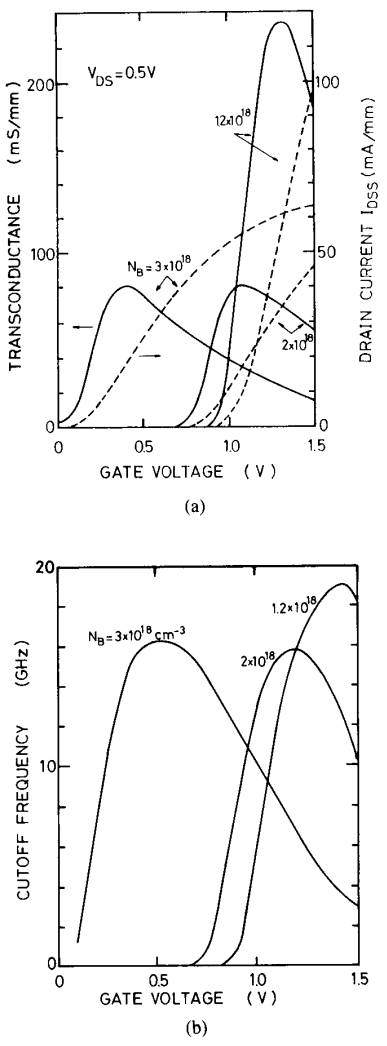

Fig. 14. FET characteristics of the 2DEG-HBT with the n-AlGaAs doping level N_B as a parameter. (a) Transconductance (solid line) and drain saturation current (dashed line) versus gate voltage. (b) Cutoff frequency versus gate voltage.

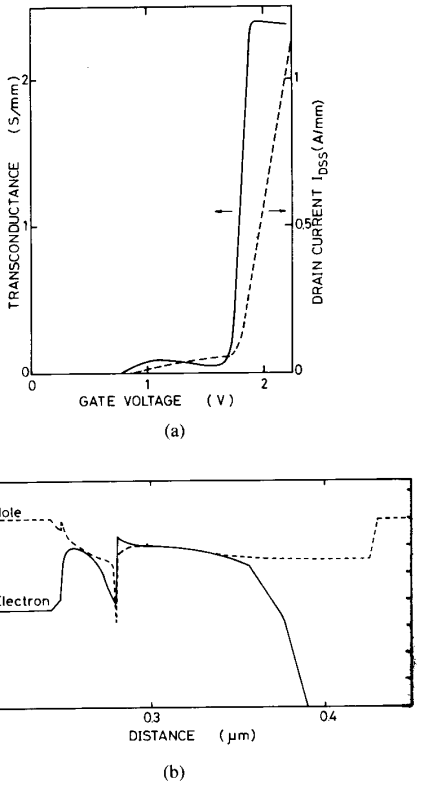

Fig. 15. FET interpretation of the bifunctional mode: extension of the FET characteristics (Fig. 8) towards larger gate voltages. (a) Transconductance (solid line) and drain saturation current (dashed line) versus gate voltage. (b) Electron (solid line) and hole (dashed line) concentration profiles versus distance from the mid-gate area near the base, for $V_G = 2$ V and a collector current density of 5×10^5 A/cm^2.

shown in Fig. 5. However, the maximum cutoff frequency is 225 GHz for collector current densities of 2×10^4 to 10^5 A/cm^2, instead of 163 GHz for the bipolar mode. The emitter-to-collector delay time is less than that of the standard bipolar operation, i.e., 0.75 ps versus 1 ps.

This bifunctional operation could in principle be applied to any bipolar transistors. However, effective modulation of the channel (base) in the FET mode would prevents protection against punchthrough of the neutral base (channel) in the bipolar mode. This limitation does not apply to the 2DEG-HBT as it has no neutral base.

V. Discussions

This section discusses the base resistance r'_{bb}, the maximum oscillation frequency f_{max}, the limitation of the classical simulator.

A. Base Resistance r'_{bb} and Maximum Oscillation Frequency f_{max}

One of the advantages of the bipolar transistor is the base resistance r'_{bb}, which depends on the extrinsic shape of the transistor.

The main task of the device design is to achieve a device structure with a low base resistance r'_{bb}, keeping the current gain h_{FE} and f_T as high as possible.

In this section we comment on a simple estimation of the base resistance r'_{bb} with an assumption that the intrinsic base resistance at high collector currents can be estimated to be 10 Ω from the 1-kΩ/□ 2DEG sheet density. This assumption gives an estimated base resistance r'_{bb} of 20 Ω, which value is one order of magnitude smaller than that of the advanced Si bipolar transistors [12].

Assuming 20 Ω for the base transistance r'_{bb}, the maximum oscillation frequencies f_{max} can be estimated to be 40 GHz for the "central structure" of Fig. 2 and Table II, and 103 GHz for the SiO_2-embedded structure, in which the maximum oscillation frequency f_{max} can be estimated by the conventional formula

$$f_{max} = \sqrt{f_T/8\pi r'_{bb} C_{BC}}. \tag{9}$$

The base-collector capacitances C_{BC} are 110 and 30 fF for both structures, respectively. As the intrinsic base-collector capac-

itance C_{BC}^{i} for the "central structure" is 7.7 fF, the real base-collector capacitance C_{BC} can be reduced by shrinking the extrinsic base-collector region. In this case, the intrinsic maximum f_{max} is almost 200 GHz.

B. Limitations of the Present Simulator

1) Quantum Effects: One of the main questions regarding the applicability of the classical simulator to the 2DEG-HBT is to what extent can the simulator quantitatively describe the vertical and horizontal motion of the 2DEG.

As was previously noted in Section II, the present simulator has successfully demonstrated [5] that the sheet number of the 2DEG at the n-AlGaAs/undoped GaAs heterointerface can be quantitatively described by introducing the *DX* center model in n-AlGaAs. It also shows that the horizontal motion of the 2DEG along the heterointerface is well described to explain the experimental data of the HEMT characteristics. However, the classical simulator cannot describe the real shape of the vertical distribution of electrons at the AlGaAs/GaAs heterointerface due to the quantum effects [13]. One of the distinctive features of the 2DEG-HBT is that the base is formed in the undoped semiconductor layer (VI) of Fig. 2 and Table II, which is separate from the original doped layer, n-AlGaAs, (IV). The 2DEG-HBT could control the vertical distribution of the 2DEG by the electric field through the base-collector voltage V_{BC}. However, the quantum-mechanical description of the vertical distribution of the 2DEG is inevitably beyond the classical description.

The vertical motion of the 2DEG through the AlGaAs/GaAs heterointerface cannot be quantitatively described by the classical simulator because the transition probabilities of electrons and holes through the heterointerface should be determined by quantum mechanics. Generally speaking, the real base current I_B and the current gain h_{FE} are thought to be affected by the recombination rate of the minority carriers at the surface or junction, and the transition rate through the heterointerface, so that it is not an easy task to simulate quantitatively the real base current or the current gain.

2) Overshoot Effect of Holes: The present classical simulator models the behavior of light holes and heavy holes under the high electric field by introducing one saturation velocity V_s for both holes. The motion of light and heavy holes under the high electric field is a key factor in the bipolar operation of the 2DEG-HBT's. In the case of n-p-n HBT's, the specific collector structure [14] has demonstrated the overshoot effect of electrons. The overshoot effect of the light hole was recently reported in a low-temperature hot hole transistor structure [15]. If the overshoot effect of holes takes place at room temperature, this simulator could incorporate phenomenologically the overshoot effect by assigning a larger value to the saturation velocity V_s.

Regarding the surface recombination effects on the base current, the experiment [16] and the simulation [17] showed that the surface recombination effect is the limiting factor of current gain h_{FE}. Even though full understanding of the surface recombination is incomplete, this simulator can incorporate phenomenologically the recombination term in the surface or junction area.

VI. Conclusions

This study has demonstrated the device concept and the bipolar operation of the two-dimensional electron gas base HBT (2DEG-HBT). Simulation shows the base transit time to be negligible and the emitter-to-collector delay time is limited mostly by the base-collector depletion layer transit time. For the bipolar operation, a cutoff frequency f_T of 163 GHz and maximum oscillation frequency f_{max} of 100 GHz are predicted for an ideal device structure with an SiO_2-embedded structure with an emitter size of 1 μm $\times$ 10 μm. Optimization of the epitaxial layer structure enables the tradeoffs for the design of a higher performance FET (e.g., G_m = 235 mS/mm and f_T = 19 GHz for L_g = 1 μm) without sacrificing of the bipolar function.

As for the bifunction operation, biasing the drain with respect to the source, the bipolar mode shows an extremely high cutoff frequency f_T of 225 for the embedded SiO_2 structure.

The 2DEG-HBT can easily achieve monolithic integration on p-n-p HBT and 2DEG-FET (or HEMT: Schottky-gate 2DEG-FET) by the same epitaxial multi-layer structures. This merged integrated structures of 2DEG-HBT are promising for future high-speed and low-power BiCMOS-like GaAs LSI's.

Acknowledgment

The authors wish to thank Dr. H. Matsumura for his continuing encouragement.

References

[1] T. Usagawa, S. Goto, T. Mishima, M. Yamane, M. Kobayashi, M. Kawata, and S. Takahashi, "A new two-dimensional electron gas base transistor (2DEG-HBT)," in *IEEE IEDM Tech. Dig.*, pp. 78–81, Dec. 1987.

[2] T. Mimura, S. Hiyamizu, T. Fujii, and K. Nanbu, "A new field effect transistor with selectivity doped GaAs/$Al_xGa_{1-x}As$ heterojunctions," *Japan J. Appl. Phys.*, vol. 19, pp. L225–L227, 1980.

[3] T. Ishikawa, J. Saito, S. Sasa, and S. Hiyamizu, "Electrical properties of Si-doped $Al_xGa_{1-x}As$ layers grown by MBE," *Japan J. Appl. Phys.*, vol. 21, pp. L675–L676, 1082.

[4] T. Ohtoshi, K. Yamaguchi, C. Nagaoka, T. Uda, Y. Murayama, and N. Chinone, "A two-dimensional device simulator of semiconductor lasers," *Solid-State Electron.*, vol. 21, pp. 627–638, 1987.

[5] H. Mizuta, K. Yamaguchi, M. Yamane, T. Tanoue, and S. Takahashi, "Two-dimensional numerical simulation of Fermi-level pinning phenomena due to *DX* centers in AlGaAs/GaAs HEMT's," *IEEE Trans. Electron Devices*, vol. 36, pp. 2307–2314, 1989.

[6] J. Yoshida, M. Kurata, K. Morizuka, and A. Hojo, "Emitter-base bandgap grading effects on AlGaAs/GaAs heterojunction bipolar transistor characteristics," *IEEE Trans. Electron Devices*, vol. ED-32, pp. 1714–1721, 1985.

[7] D. A. Sunderland and P. D. Dapkus, "Optimizing n-p-n and p-n-p heterojuction bipolar transistors for speed," *IEEE Trans. Electron Devices*, vol. ED-34, pp. 367–377, 1987.

[8] G. W. Taylor and J. G. Simmons, "Bipolar inversion channel field effect transistor," *IEEE Trans. Electron Devices*, vol. ED-32, pp. 2345–2367, 1985.

[9] M. Meyyapan, J. P. Kreskovsky, and H. L. Grubin, "Numerical Simulation of an AlGaAs/GaAs bipolar inversion channel field effect transistor," *Solid-State Electron.*, vol. 26, pp. 1023–1030, 1988.

[10] H. Kroemer, "Heterojunction bipolar transistors and integrated circuits," *Proc. IEEE*, vol. 70, pp. 64–76, 1982.

[11] K. Matsumoto, Y. Hayashi, T. Kojima, T. Nagata, and T. Yoshimoto, "Integration of GaAs SISFET and GaAs inversion-base bipolar transistor," in *Extended Abstracts 20th Conf. on Solid State Devices and Materials*, pp. 531–534, 1988.

[12] T. Nakamura, K. Ikeda, N. Kakazato, K. Washio, M. Namba, and T. Hayashida, "63 ps ECL circuits using advanced SICOS technology," in *IEEE IEDM Tech. Dig.*, pp. 472–475, Dec. 1986.

[13] T. Ando, "Self-consistent results for a GaAs/AlGaAs heterojunction. I. Subband structure and light-scattering spectra," *J. Phys. Soc. Japan*, vol. 51, pp. 3893–3899, 1982.

[14] T. Ishibashi and Y. Yamauchi, "A possible near-ballistic collection in an AlGaAs/GaAs HBT with a modified collector structure," *IEEE Trans. Electron Devices*, vol. 35, pp. 401-404, 1988.
[15] M. Heiblum, "Ballistic transport of electrons and holes," in *IEEE IEDM Tech. Dig.*, pp. 822-825, Dec. 1988.
[16] O. Nakajima, K. Nagata, H. Ito, T. Ishibashi, and T. Sugeta, "Emitter-base junction size effect on current gain Hf_e of AlGaAs/GaAs heterojunction bipolar transistors," *Japan J. Appl. Phys.*, vol. 24, pp. L596-598, 1985.
[17] Y. Someya Hiraoka, J. Yoshida, and M. Azuma, "Two-dimensional analysis of emitter-size effect on current gain for GaAlAs/GaAs HBT's," *IEEE Trans. Electron Devices*, vol. ED-34, pp. 721-725, 1987.

*

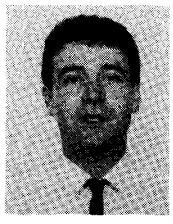

Patrick D. Rabinzohn was born in Belley, France, on February 19, 1958. He graduated as an Engineer from the "Ecole Supérieure d'Electricité," Gif-sur-Yvette, France, in 1981, and received the Ph.D. degree in material science from "Pierre et Marie Curie" University, Paris, France, in 1983.

In 1984, he joined the "Laboratorie d'Electronique Philips," Limeil-Brévannes, France. From 1984 to 1987 he worked in the research and development of GaAs MMIC's and dry etching processing for GaAs IC's technologies. As an Exchange Researcher from the Philips Research Organization, he was in 1988 a Visiting Researcher at the Central Research Laboratory, Hitachi Ltd., Tokyo, Japan, where he worked on research and development of new compound semiconductor electron devices. In 1989, at L.E.P., he was supervising research and development on III-V devices and IC's processing. In November 1989, he joined Matra MHS, Nantes, France, as a member of the engineering department.

*

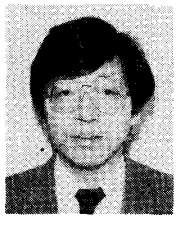

Toshiyuki Usagawa was born in Yamaguchi, Japan, in 1953. He received the B.S., M.S., and Ph.D. degrees, all in physics, from the University of Tokyo, Tokyo, Japan, in 1976, 1978, and 1981, respectively. His thesis subject was the theoretical work on Spin Dynamics with Relaxation of Superfluid ^{3}He.

In 1981, as a Research Fellow of Japan Society for the Promotion of Science, he was involved in the group-theoretical analysis of the antiferromagnetic ordered nuclear spins of solid ^{3}He. He joined the Central Research Laboratory, Hitachi, Ltd., in 1982, and has been working in the field of GaAs/AlGaAs heterojunction high-speed devices. He has been involved in the deep-recessed gate structure of 2DEG-FET and 2DEG-HBT. His current interests are in mesoscopic electronics and the electrooptic merged devices of the III-V materials.

Dr. Usagawa is a member of the Physical Society of Japan and the Japan Society of Applied Physics.

*

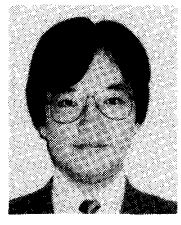

Hiroshi Mizuta (M'89) was born in Kochi, Japan, in 1961. He received the B.S. and M.S. degrees in physics from Osaka University, Osaka, Japan, in 1983 and 1985, respectively.

He joined the Central Research Laboratory, Hitachi Ltd., Tokyo, Japan, in 1985, and has been engaged in research on two-dimensional numerical simulation of heterojunction devices, and modeling of new functional devices. Since June 1989, he has been working in the field of quantum interference devices at the Hitachi Cambridge Laboratory, Hitachi Europe Ltd., Cambridge, England.

Mr. Mizuta is a member of the Physical Society of Japan, the Japan Society of Applied Physics, and the Electron Devices Society of the IEEE.

*

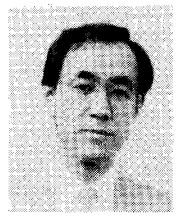

Ken Yamaguchi (M'76) was born in Tokyo, Japan, in 1947. He received the B.Sc. and M.Sc. degrees from Yokohama National University, Yokohama, Japan, in 1970 and 1972, respectively, and the Ph.D. degree from the University of Tokyo, Tokyo, Japan, in 1980, all in electrical engineering.

He joined the Central Research Laboratory, Hitachi Ltd., in 1972, and has been working in the field of semiconductor device design technologies. His current research interests are in device physics, device modeling, simulation technologies, and CAD systems for designing semiconductor devices and circuits.

Dr. Yamaguchi is a member of the Physical Society of Japan, the Japan Society of Applied Physics, the Institute of Electronics, Information and Communication Engineers of Japan, and the Electron Devices Society of the IEEE.